GSA DATA REPOSITORY 2014296

Supplementary material

Splay fault activity revealed by aftershocks of the 2010 Mw=8.8 Maule earthquake, Central Chile

Lieser, K., Grevemeyer, I., Lange, D., Flüh, E., Tilmann, F., and Contreras-Reyes, E.

Contents

1 FIGURES

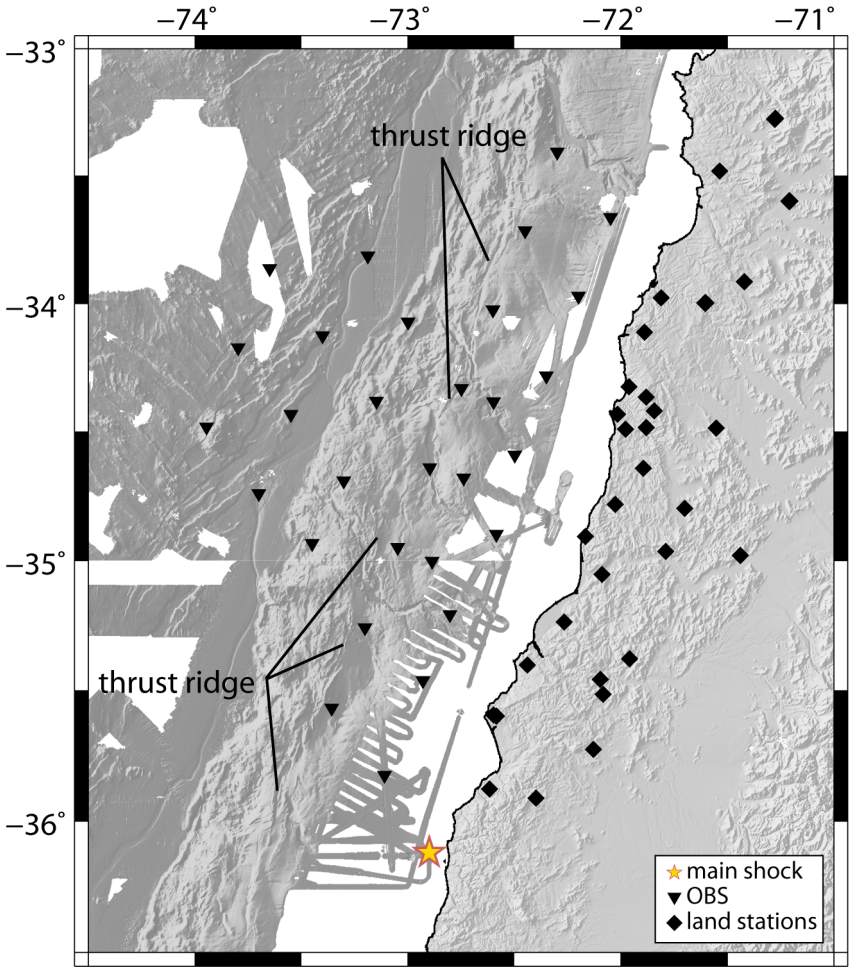

Figure DR1: Map of station configuration.

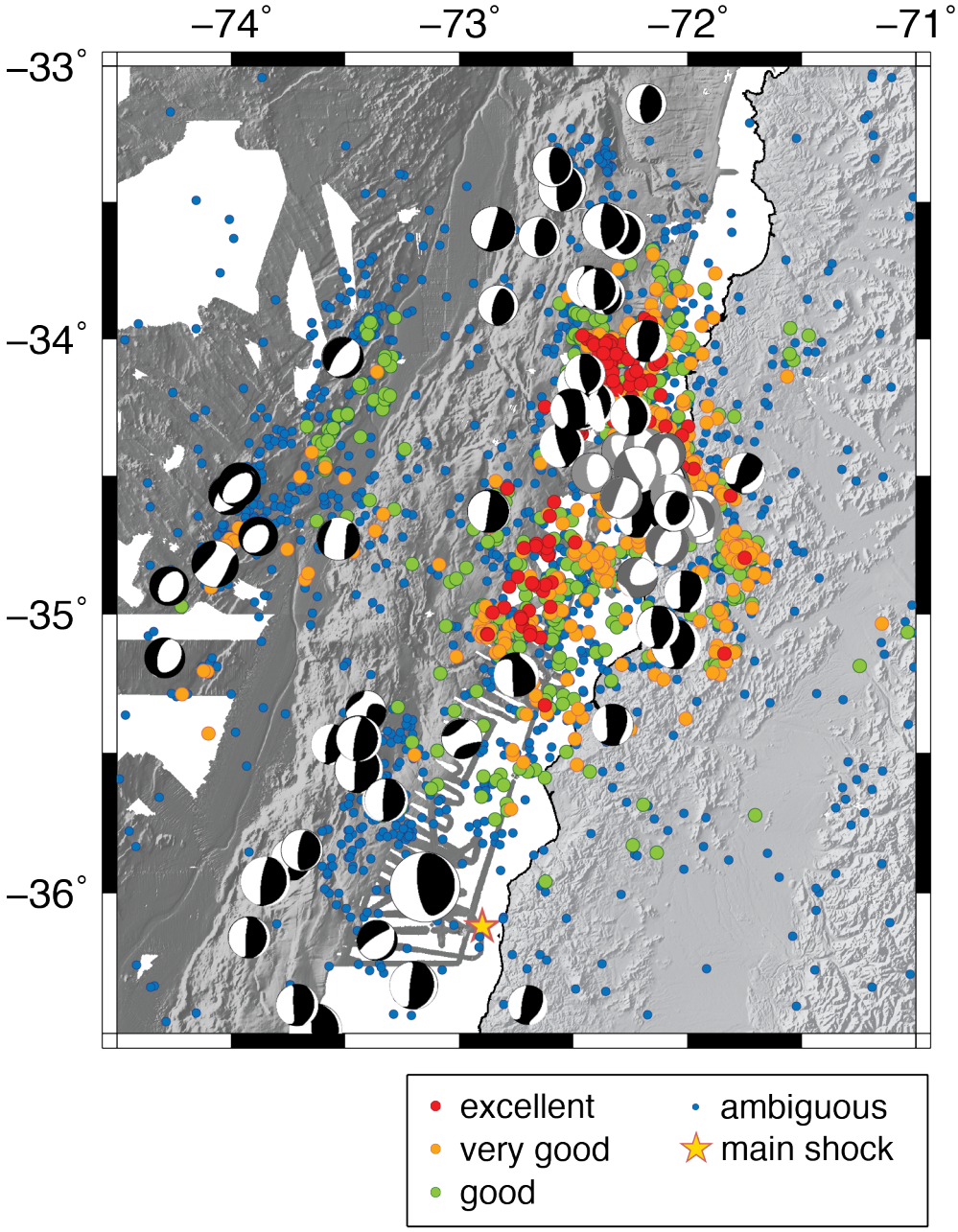

Figure DR2: Map with aftershocks of the Maule event from September to December 2010 from the local amphibious network and focal mechanisms with hypocenters from the gCMT catalog (Dziewonski et al., 1981; Ekström et al., 2012) from February to December 2010 . Events with extensive focal mechanisms of the Pichilemu cluster are shown in gray. Size of focal mechanisms is relative to magnitude.

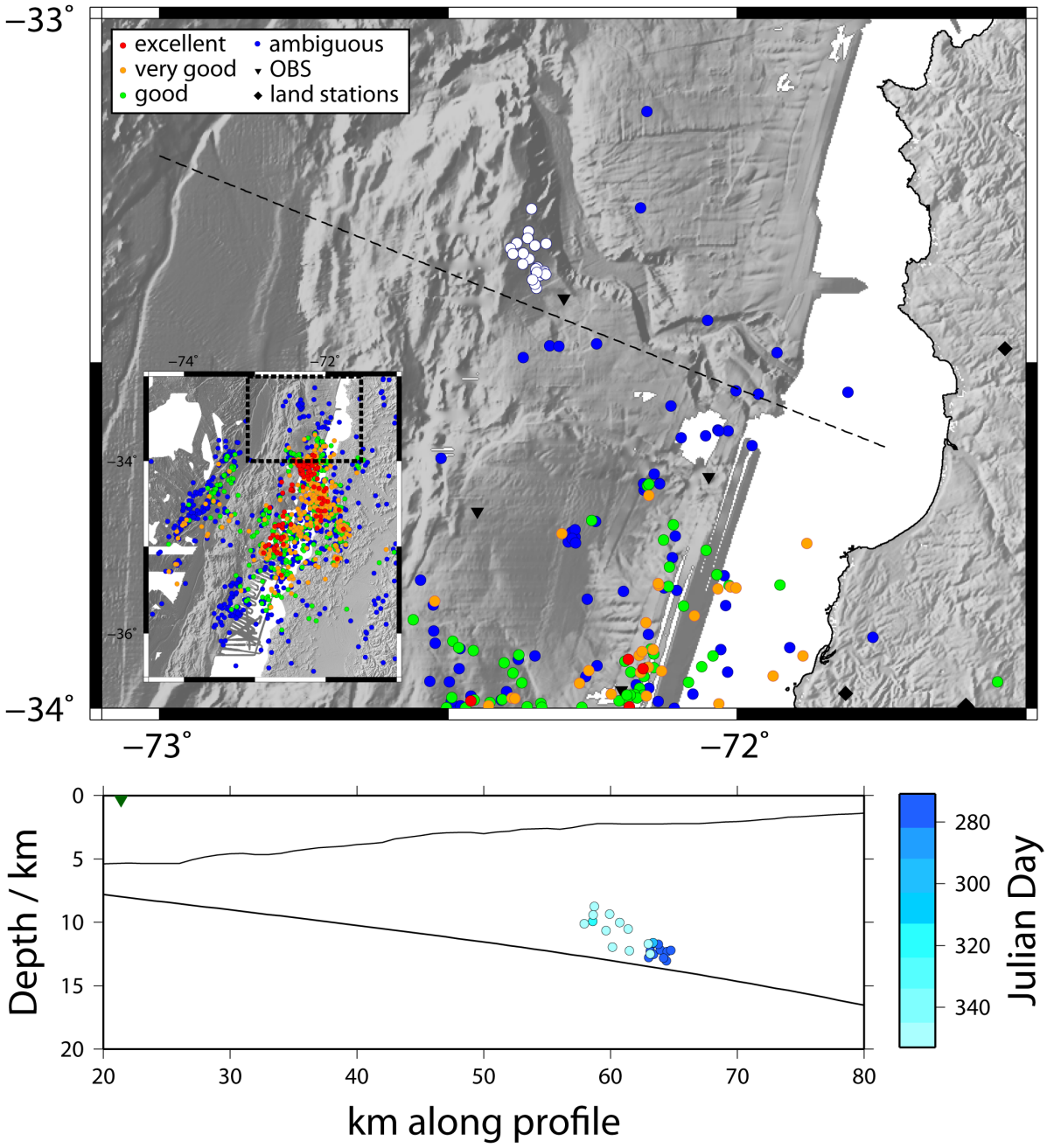

Figure DR3: Cluster, highlighted in white, at the northern boundary of the survey area and projected onto a cross-section perpendicular to the trench. Quality class "ambiguous" was restricted to the maximum average error within the cluster of 23 km (see Table DR2). Cluster events in the cross-section are color coded by origin time showing two episodes of faulting with a first set of events nucleating within two days at the end of September and a second one originating within three days at the end of December (October 1., 2010 = 274 Julian day; November 1., 2010 = 305 Julian day; December 1. ,2010 = 335 Julian day). Plate boundary by Slab1.0 model (Hayes et al., 2012).

2 AUTOMATIC P WAVE PICKING AND EVENT LOCATION

Event detection was carried out with a STA/LTA trigger and a coincidence criterion leading to 4,592 events. The picking of P wave onsets was performed with the automatic P wave picking engine MPX by Aldersons (2004), whose parameters have to be tuned to the data set. At first, the program requires an initial pick time near the P wave onset, usually an existing manual pick or a calculated onset based on catalog locations and a chosen velocity model. Since neither exists, the traces of each station per event were analyzed again by the STA/LTA trigger with adapted parameters in order to get the initial pick. Trigger parameters were optimized to obtain as many P wave onsets as possible but also as little noise, spikes, and S wave onsets as possible. Most of the initial picks not related to a P wave onset are not recognized by MPX. However, multiple picked onsets in a single seismogram occur and have been evaluated before event location as follows: the event is located with HYPOCENTER 3.2 (Lienert and Havskov, 1995) which calculates the residual for every onset. The one with the least residual is considered to be the correct pick. Stations where only a single pick was made but did not detect the correct onset will be automatically weighted down in the final event location. Trigger and MPX picking parameter were optimized for both OBS and land station network separately and tested on a reference data set consisting of 44 events. The 75% percentile of the absolute difference between manual and automatic picks for the OBS network was 0.09 s and for the land station network 0.08 s (Table DR1). MPX is also able to classify

the quality of an onset which will have an effect on event location since onsets with lower qualities will be weighted down. In order to adapt this classification scheme a reference data set was picked both automatically as well as manually followed by a hypocenter determination. For the final scheme the 75% percentiles were in the range of 2.3 - 5 km for deviations in longitude, latitude and depth for the OBS network. Deviations for the land stations showed 75% percentiles with values in the range of about 0.5 - 2 km in all three directions. 67,454 P wave onsets could be identified by MPX in its final setting.

The event localization was performed by NonLinLoc (Lomax, 2011), a probabilistic, global-search earthquake location software. Since 1-D velocity models provided either good results for the onshore or the offshore domain but only poor results for the whole survey area, a 2.5-D model was generated. Results from a seismic refraction and wide-angle profile crossing the network (Moscoso et al., 2011) defined the offshore domain and coastal region while constraints from a local earthquake study between 34°S and 36°S (Kraft, 2011; Dannowski et al., 2013) defined the domain onshore (DR4). The upper part of the subducting slab until about 20 km depth was constrained by the results of the seismic refraction and wide-angle profile and due to decreasing depth resolution of the refraction seismic data below 20 km depth the slab was defined by the Slab1.0 model of Hayes et al. (2012) for larger depths. By stretching this 2-D model along the geometry of the trench a 2.5-D model was set up. NonLinLoc determines a maximum likelihood hypocenter based on the probability density function (PDF) calculated for each event. From the PDF scatter samples a 3-D 68% confidence error ellipsoid and an expected hypocenter are estimated. Based on those parameters the located events were classified into five quality categories (see Table DR2, after Husen and Smith, 2004). Several sequential location runs were performed to determine station corrections, which were set to the average residuals at each station in the previous run. In total 3,751 of the triggered events could be located and 1,043 events were classified as “good” or better.

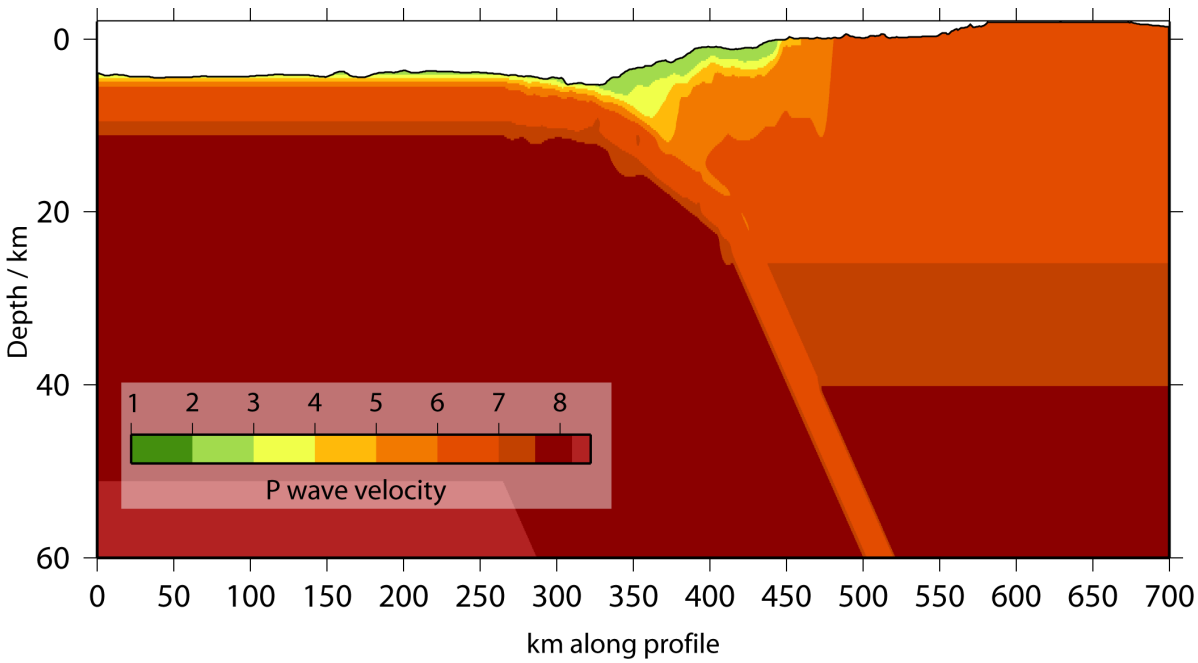

Figure DR4: Upper 60 km of velocity model used for event location derived by seismic refraction and wide-angle profile crossing the network (Moscoso et al., 2011) and a local earthquake study (Kraft, 2011; Dannowski et al., 2013).

ADDITIONAL REFERENCES

Lienert, B.R., and Havskov, J., 1995, A computer program for locating earthquakes both locally and globally: Seismological Research Letters, v. 66, no. 5, p. 26–36, doi:10.1785/gssrl.66.5.26.

TABLE DR1. DEVIATIONS BETWEEN MANUALLY AND AUTOMATICALLY PICKED DATA SETS

Percentiles	Picking time	Hypocenter location		
		Latitude	Longitude	Depth
	(s)	(km)		
OBS				
25%	0.01	0.18	0.40	0.00
50%	0.04	0.36	0.75	0.63
75%	0.09	2.28	4.89	3.09
Land stations				
25%	0.01	0.00	0.28	0.58
50%	0.03	0.42	0.69	1.29
75%	0.08	0.85	1.51	2.03

Table DR1: Deviations in picking time and hypocenter location between manually and automatically picked data sets.

TABLE DR2. QUALITY CLASSES FOR EARTHQUAKE LOCATIONS

Class	RMS (s)	Distance (km)	Average error (km)	Number of events
A – excellent	< 0.5	< 0.5	< 2	145
B – very good	< 0.5	< 0.5	≥ 2	370
C – good	< 0.5	0.5 – 2	< 5	528
D – ambiguous	< 0.5	≥ 0.5*	-	1689
E – poor †	> 0.5	-	-	1019

* Except class C
† Not displayed in figures.

Table DR2: Quality classes for earthquake locations (after Husen and Smith, 2004). "Distance" is the difference between the maximum likelihood and the expectation hypocenter location and "Average error" is the mean of the three axes of the 68% error ellipsoid from NonLinLoc.

3 CRITICAL COULOMB WEDGE THEORY

The critical Coulomb wedge theory considers accretionary wedges as similar to wedges of soil or snow generated by a bulldozer and was successfully applied to convergent margins (e.g. Wang and Hu, 2006; Cubas et al., 2013). We will briefly describe the main equations and refer the reader to Dahlen (1990) and Davis et al. (1983) for further reading.

For a critical wedge the following equation is valid:

$$\alpha + \beta = \Psi_B - \Psi_0 \tag{3.1}$$

where Ψ_B is the angle between the maximum principal stress σ_1 and basal slope, Ψ_0 is the angle between surface slope and σ_1, α and β describe the angles between the horizontal and surface slope and the base of the wedge, respectively (Fig. DR5).

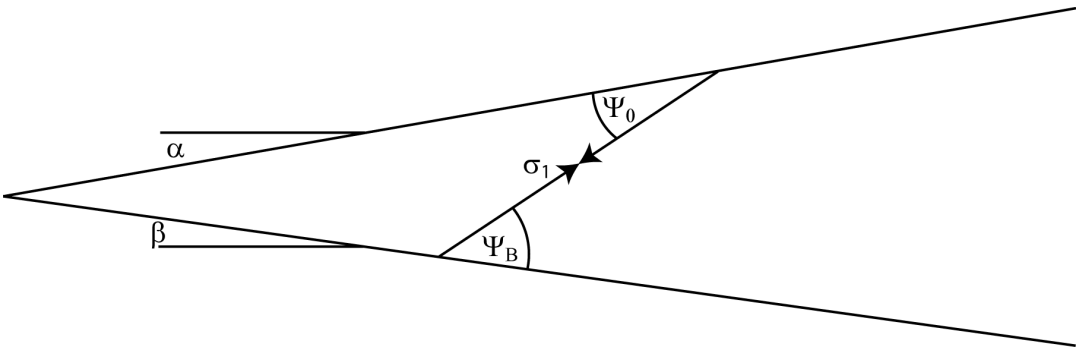

Figure DR5: Sketch of a wedge with the angles α, β, Ψ_B and Ψ_0.

The angles $\Psi_{B,0}$ are:

$$\Psi_B = \frac{1}{2}\arcsin\left(\frac{\sin\phi_b^{'}}{\sin_{int}}\right) - \frac{1}{2}\phi_b^{'} \tag{3.2}$$

and

$$\Psi_B = \frac{1}{2}\arcsin\left(\frac{\sin\alpha^{'}}{\sin_{int}}\right) - \frac{1}{2}\alpha^{'} \tag{3.3}$$

where

$$\tan\phi_b^{'} = \left(\frac{1-\lambda_b}{1-\lambda}\right)\tan\phi_b = \frac{\tan\Phi_b^{EFF}}{1-\lambda} \tag{3.4}$$

with $\tan\phi_b^{EFF} = (1-\lambda_b\tan\phi_b)$ (Cubas et al., 2013) and

$$\alpha^{'} = \arctan\left[\left(\frac{1-\rho_w/\rho}{1-\lambda}\right)\tan\alpha\right], \tag{3.5}$$

where λ is the pore pressure ratio and ρ is the density of water and of rock, respectively. The angles ϕ_{int} and ϕ_b are internal and basal friction angles with $\mu_{int,b} = \tan\phi_{int,b}$. Values for ϕ_{int}, λ and ϕ_b^{EFF} for outer and inner wedge were taken from Cubas et al. (2013) and ρ was set to 3000 kg/m^3. Calculating β for a set of given α with equation 3.1 with different parameter for the inner and outer wedge leads to the critical envelopes in the stability diagram in Figure DR6. Inside the envelopes the wedge is in a stable state whereas outside it is in an unstable state and along the branches of the envelope in a critical state and at the verge of failure.

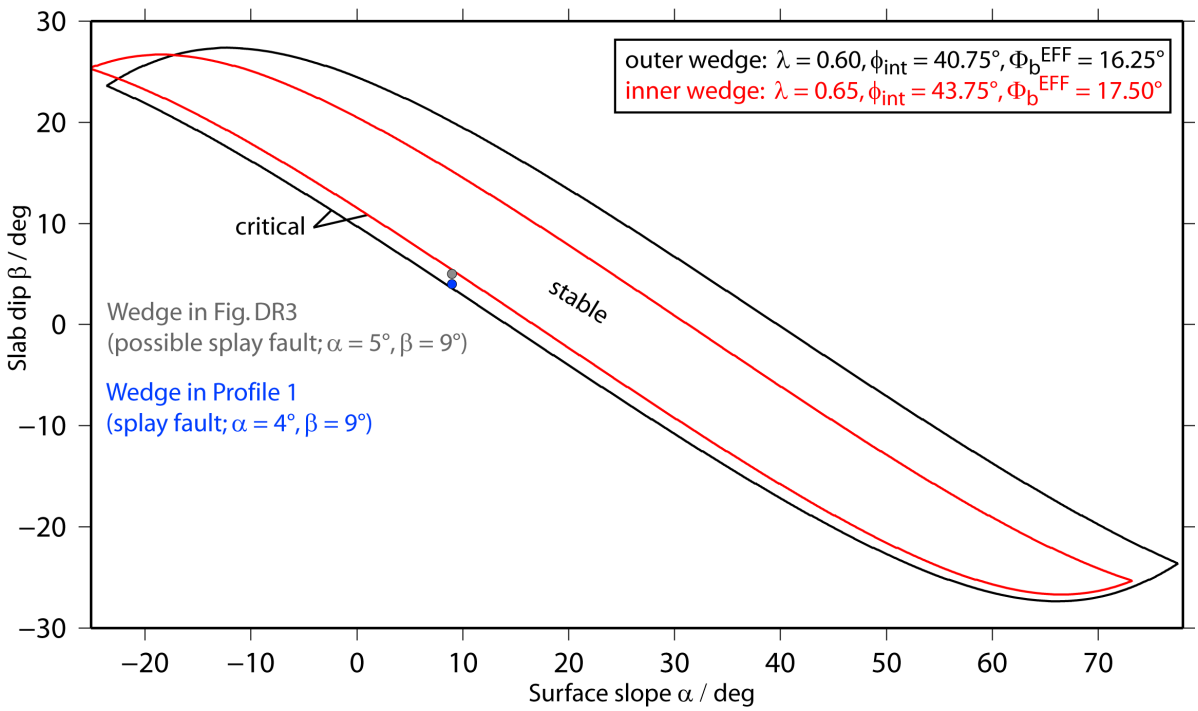

Figure DR6: Stability diagram for the outer and inner wedge in the northern deployment area. The blue dot marks the taper corresponding to the splay fault region and the grey dot marks the taper for where the cluster at the northern boundary of the deployment area is located. Parameter for outer and inner wedge according to Cubas et al. (2013).